"Double-Cable" conjugated polymers with linear backbone toward high quantum efficiencies in single-component polymer solar cells

"Double-Cable" Conjugated Polymers with Linear Backbone toward High Quantum Efficiencies in Single-Component Polymer Solar Cells

Guitao Feng,[†,±] Junyu Li,[‡] Fallon J. M. Colberts,[§] Mengmeng Li,[§] Jianqi Zhang,[⊥] Fan Yang,[†,±] Yingzhi Jin,[∥] Fengling Zhang,[∥] René A. J. Janssen,[§] Cheng Li[†] and Weiwei Li*[,†]

[†]Beijing National Laboratory for Molecular Sciences, Key Laboratory of Organic Solids, Institute of Chemistry, Chinese Academy of Sciences, Beijing 100190, P. R. China.

[‡]DSM DMSC R&D Solutions, P.O. Box 18, 6160 MD Geleen, The Netherlands.

[§]Molecular Materials and Nanosystems & Institute for Complex Molecular Systems, Eindhoven University of Technology, P.O. Box 513, 5600 MB Eindhoven, The Netherlands.

[⊥]National Center for Nanoscience and Technology, Beijing 100190, P. R. China.

[∥]Biomolecular and Organic Electronics, Department of Physics, Chemistry and Biology, Linköping University, SE-581 83, Linköping, Sweden.

[±]University of Chinese Academy of Sciences, Beijing 10049, P. R. China.

Abstract

A series of "double-cable" conjugated polymers were developed for application in efficient single-component polymer solar cells, in which high quantum efficiencies could be achieved due to the optimized nanophase separation between donor and acceptor parts. The new double-cable polymers contain electron-donating poly(benzodithiophene) (BDT) as linear conjugated backbone for hole transport and pendant electron-deficient perylene bisimide (PBI) units for electron transport, connected via a dodecyl linker. Sulfur and fluorine substituents were introduced to tune the energy levels and crystallinity of the conjugated polymers. The double-cable polymers adopt a "face-on" orientation in which the conjugated BDT backbone and the pendant PBI units have a preferential π-π stacking direction perpendicular to the substrate, favorable for interchain charge transport normal to the plane. The linear conjugated backbone acts as a scaffold for the crystallization of the PBI groups, to provide a double-cable nanophase separation of donor and acceptor

phases. The optimized nanophase separation enables efficient excition dissociation as well as charge transport as evidenced from the high, up to 80%, internal quantum efficiency for photon-to-electron conversion. In single-component organic solar cells the double-cable polymers provide power conversion efficiency up to 4.18%. This is one of the highest performances in single-component organic solar cells. The nanophase separated design can likely be used to achieve high performance single-component organic solar cells.

1. Introduction

Single-component polymer solar cells (SCPSCs) have been widely studied in the last two decades.[1-5] In SCPSCs, covalently linked electron donor and acceptor parts in one material are used to absorb sunlight and generate excitons, which then diffuse towards the donor/acceptor interface, where charges are generated that can be transported to the electrodes. This photon-to-electron conversion process is usually accomplished by two materials, e.g. a donor polymer and fullerene acceptor, blended in a bulk-heterojunction (BHJ) solar cell.[6] A single photoactive material can simplify the device fabrication for SCPSCs and improve the cell stability, increasing the applicability for large-area devices.[7] Conjugated polymers designed for SCPSCs consist of block copolymers,[3] such as rod-rod[8-16] and rod-coil structures,[16-22] and "double-cable" polymers comprising a conjugated backbone as donor for hole transport with interacting pendant acceptor groups that ensure electron transport .[23-33] Although they have been successfully applied into SCPSCs, the power conversion efficiencies (PCEs) are always below 3%.[8,29,33] This is far away from the PCEs of BHJ solar cells that are now exceeding 13%,[34] leaving much room for improvement.

The dimension of the phase separation of the photoactive layer has a significant impact on the charge generation, photocurrent and PCEs in organic solar cells.[6,35-38] Due to their short lifetime, photo-generated excitons can only diffuse over small distances towards the donor/acceptor interface and, hence, an intimately mixed blend is preferred.[39] On the other hand, transport of separated free charges (holes and electrons) towards the electrodes is more efficient in large-phase separated systems, in which the smaller interfacial area reduces the probability for hole-electron recombination.[40] In order to

balance the contradicting morphological requirements for these two processes, nanophase separation with domain sizes of 10 – 20 nm is considered as the optimal morphology for high performance organic solar cells.[41-42] In BHJ systems, this can be achieved via tuning the donor/acceptor structures, such as adjusting crystallinity,[43-47] solubility[48-49] and miscibility,[50-53] and also through the device fabrication by using high-boiling point solvent additives[54] and thermal/solvent annealing methods.[45,55-57] However, the optimized blend morphology may not be stable with time or temperature. In a single conjugated polymer that contains electron donor and acceptor segments, nanophase separation is also vital to the device performance, but morphology is thermodynamically stable. Interestingly, although conjugated block copolymers can form organized nanostructures, their SCPSCs always have shown disappointing performance.[58] One reason is the limited materials selection. A frequently used donor segment in conjugated block copolymers is poly(3-hexylthiophene) because it can be obtained via a catalyst-transfer polycondensation.[59-62] This quasi-living polymerization provides oligothiophenes with controlled end groups and molecular weight, which can be used to prepare block copolymers. By comparison, double-cable conjugated polymers can be constructed from a vast amount of donor polymers and fullerene or non-fullerene acceptors.[63] In contrast to block copolymers, the conjugated backbone and the covalently bound acceptor side groups of most double cable polymers tend to form a completely mixed morphology, resulting in a poor device performance.

Recently, we reported three double-cable conjugated polymers based on a diketopyrrolopyrrole (DPP)-polymer backbone and perylene bisimide (PBI) side units.[33] We found that longer alkyl (dodecyl) linkers between DPP and PBI units improved the crystallinity of the polymers compared to the shorter alkyl (hexyl) linkers, which could be further enhanced by using alkylthiothiophene side groups. It seemed that the enhanced crystallinity in these polymers was related to the better nanophase separation, as confirmed by their high PCEs in SCPSCs. Therefore, we speculated that by rationally designing new double-cable conjugated polymers, it should be possible to further optimize the nanophase separation and adequately balance the contradictory morphological requirements for charge generation and charge transport in organic solar cells.

Herein, a new strategy to adjust the nanophase separation of double-cable polymers is reported by using a linear conjugated backbone. We propose that the linear backbone self-assembles into aligned structures, so that the acceptor side units are forced to locate in between the conjugated backbones, resulting in nanophase separation between them. The linear backbone is similar to the donor polymer PBDTT (Figure 1a), which has been reported to provide high quantum efficiencies in BHJ solar cells.[64] The backbone consists of a homopolymer of benzodithiophene (BDT) units, which provide a linear configuration as indicated by density functional theory (DFT) calculations (Figure 1d). Large aromatic PBI side groups as electron acceptor were incorporated into the polymer PBDTPBI (Figure 1c) to generate intrinsic donor-acceptor systems. Sulfur and fluorine atoms were incorporated in the BDT units in S-PBDTPBI and SF-PBDTPBI (Figure 1c), to tune the frontier energy levels and crystalline properties.[34] In this work we show that these conjugated polymers containing a linear conjugated backbone and large π-conjugated side groups form nanophase-separated domains and yield high quantum efficiencies above 0.65 in solar cells. Ultimately, a high PCE of 4.18% based on the new double-cable photoactive layer was realized, representing the highest performance for SCPSCs obtained to date.

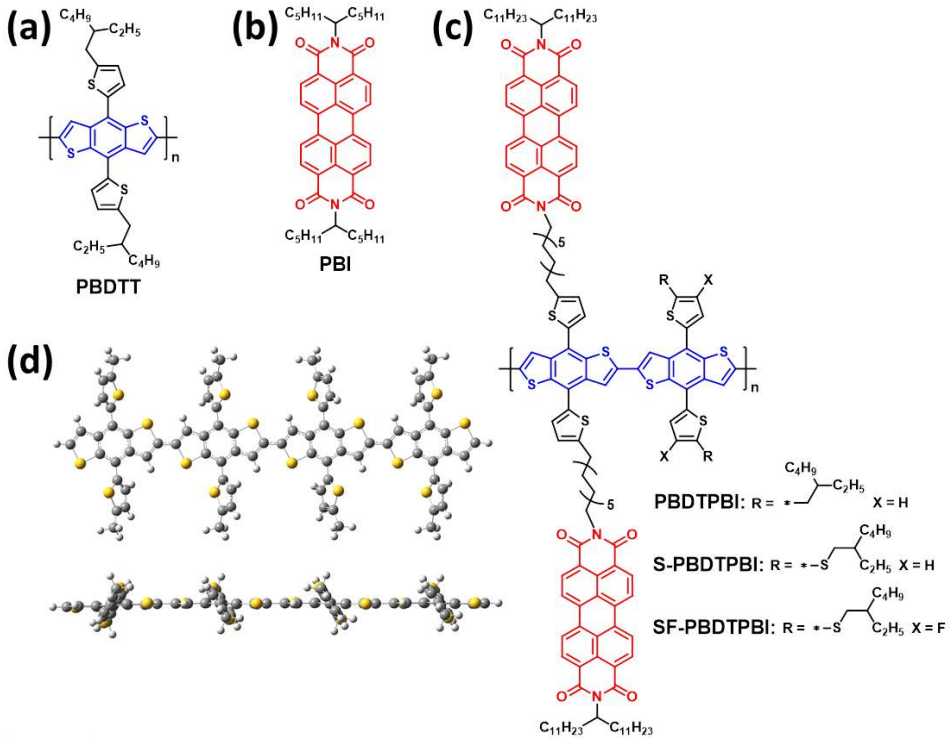

Figure 1. The chemical structures of (a) donor polymer PBDTT, (b) electron acceptor PBI and (c) double-cable conjugated polymers PBDTPBI, S-PBDTPBI, and SF-PBDTPBI. (d) Molecular geometries of PBDBT segment by DFT calculations.

2. Results

2.1. Synthesis of the monomers and polymers. The synthetic routes for the monomers and double-cable polymers are shown in Scheme 1 and the detailed procedures are described in the Supporting Information (SI). The key monomer, **M8**, is a dibromo-BDT carrying two pendant PBI units, connected via flexible dodecyl linkers. The synthesis starts by alkylating thiophene (**M1**) to yield 2-(12-bromododecyl)thiophene (**M2**). After protecting with a methoxy end group, **M3** could be used to synthesize **M4** via lithiation, reaction with benzo[1,2-b:4,5-*b'*]dithiophene-4,8-dione, and reduction with $SnCl_2$. **M4** was treated with BuLi and CBr_4 to yield **M5**, followed by reacting with HBr to yield the key precursor **M6**. The distinct reactivity of the two pairs of bromine atoms in **M6** provided the opportunity to introduce the PBI side units into monomer **M8**, while preserving the other two bromines on the BDT unit for aryl-aryl coupling polymerization reactions. In this work, we selected three distannyl-BDT compounds **M9-11** for Stille polymerization, in which the substituents attached to BDT unit varied from 2-(2-ethylhexyl)thiophene (**M9**) to 2-((2-ethylhexyl)thio)thiophene (**M10**) and 2-((2-ethylhexyl)thio)-3-fluorothiophene (**M11**).

The double-cable polymers were obtained via Stille polymerization by using $Pd(PPh_3)_4$ as catalyst and toluene/DMF as solvent. After Soxhlet extraction by acetone, hexane, and dichloromethane to remove impurities and oligomers, the polymers were isolated in a reasonable yield (64.5% - 96.3%). The polymers show good solubility in chlorobenzene (CB). The molecular weight of the new polymers was determined using gel permeation chromatography (GPC) with *o*-DCB as eluent at 140 °C. The number-average molecular weights (M_n) of PBDTPBI, S-PBDTPBI, and SF-PBDTPBI are 42.8, 37.0, and 26.3 kDa, respectively (Table 1). For reference, PBDTT was synthesized according to a literature procedure[64] and obtained with M_n = 21.0 kDa. All polymers exhibited good thermal stability with 5% weight loss temperature above 340 °C (Figure S1, SI). Differential scanning calorimetry measurement shows that the compound **PBI**

has typical melt and crystallization behavior, while PBDTT and PBDTPBIs have no thermal transition in the measurement (Figure S2).

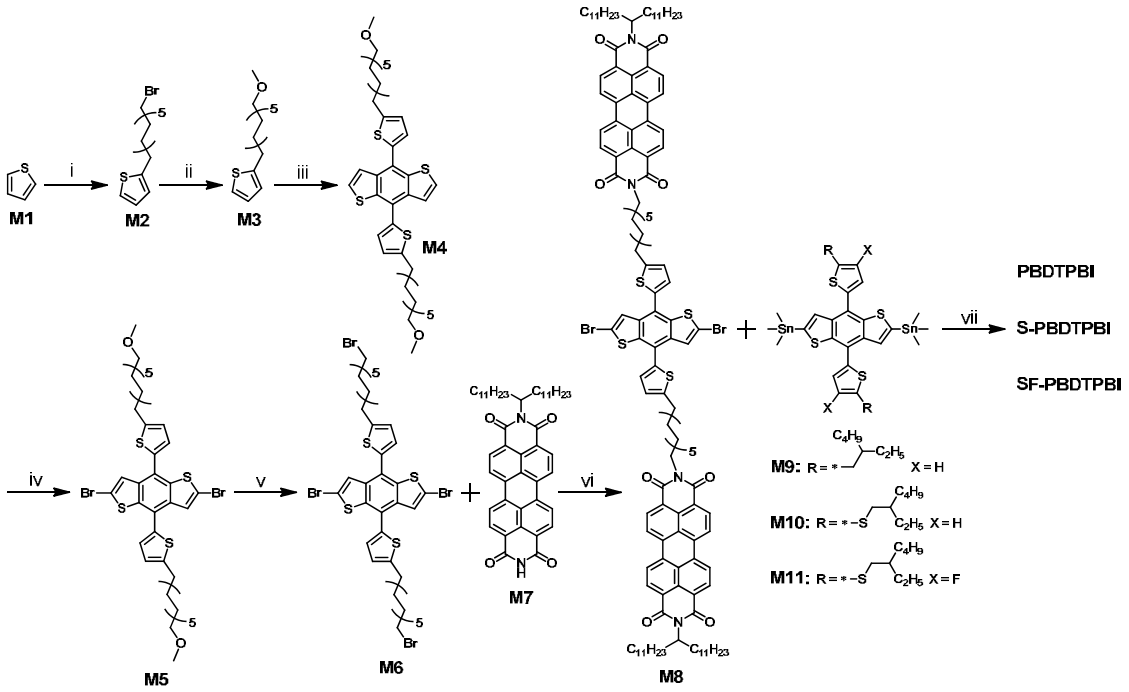

Scheme 1. Synthetic routes of the monomers and polymers. (i) n-BuLi, 0 °C, 1 h, 1,12-dibromododecane in THF at 60 °C, 12 h; (ii) $NaOCH_3$ in methanol at 90 °C, 12 h; (iii) n-BuLi at 50 °C, 1 h, benzo[1,2-b:4,5-*b'*]dithiophene-4,8-dione in THF at 50 °C, 1 h, $SnCl_2/HCl/H_2O$; (iv) BuLi, 0 °C, 30 min, r.t, 1.5 h, CBr_4, 12 h; (v) HBr, 140 °C, 12 h; (vi) K_2CO_3, in DMF at 60 °C, 48 h; (vii) Stille polymerization, $Pd(PPh_3)_4$ in toluene/DMF (10:1, v/v) at 115 °C, 24 h.

2.2. Optical and Electrochemical Properties. The UV-vis absorption spectra of the double-cable polymers in thin films (Figure 2a) and in $CHCl_3$ solution (Figure S3, SI) are similar to those of the donor polymer PBDTT and the electron acceptor **PBI** (Figure 1b). PBDTPBI and its derivatives show two peaks at 490 nm and 530 nm in thin film and solution, with a shoulder at 560 nm. The intensity of the shoulder at 560 nm is significantly enhanced in thin films, indicating that it is related to aggregation. The long-wavelength shoulder can be attributed to stacked PBI units, as a similar shoulder can be observed in the absorption of **PBI** (Figure 2a). PBDTPBIs have an optical band gap (E_g)

of 2.10 eV, which is similar to that of the donor polymer PBDTT and the PBI units (Table 1).

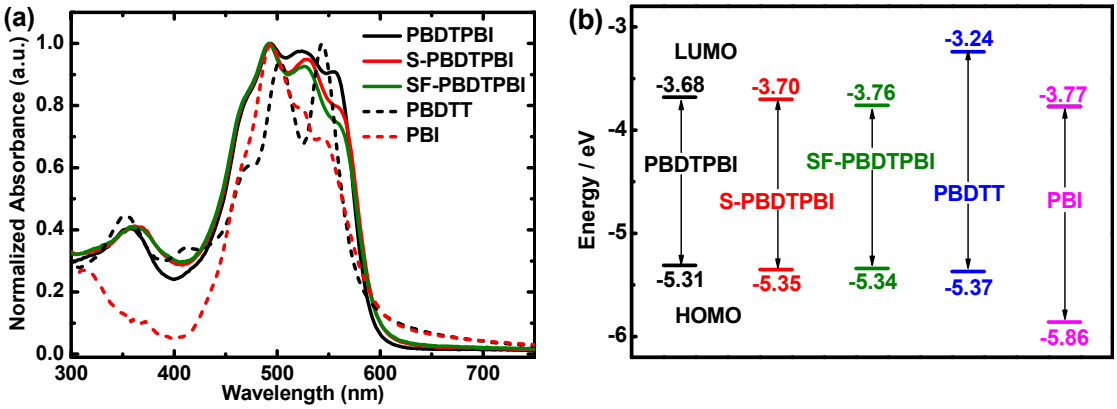

Figure 2. (a) Optical absorption spectra of the double-cable conjugated PBDTPBI polymers, PBDTT, and PBI. (b) HOMO/LUMO energy levels determined from cyclic voltammetry vs Fc/Fc^{+}.

Table 1. Molecular Weight and Optical Properties of the Polymers and PBI.

Polymer	M_n [a] (kDa)	M_w [a] (kDa)	PDI	E_g^{sol} (eV)	E_g^{film} (eV)	E_{HOMO}^{CV} (eV)	E_{LUMO}^{CV} (eV)	E_g^{CV} (eV)	E_{HOMO}^{UPS} (eV)
PBDTPBI	42.8	76.1	1.78	2.14	2.10	-5.31	-3.68	1.63	-5.16
S-PBDTPBI	37.0	66.4	1.79	2.12	2.08	-5.35	-3.70	1.65	-5.18
SF-PBDTPBI	26.3	46.8	1.78	2.10	2.08	-5.34	-3.76	1.58	-5.25
PBDTT	21.0	43.6	2.08	2.20	2.13	-5.37	-3.24	2.13	-4.99
PBI	-	0.698[b]	-	2.29	2.09	-5.86	-3.77	2.09	-6.30

[a] Determined with GPC at 140 °C using *o*-DCB as the eluent. [b] Determined by high resolution MALDI-TOF spectra.

The frontier energy levels of the polymers and **PBI** determined by cyclic voltammetry measurement (Figure S4, SI) are shown in Figure 2b. The highest occupied molecular orbital (HOMO) levels of PBDTPBIs are similar to that of PBDTT, while the lowest unoccupied molecular orbital (LUMO) levels are similar to that of **PBI**. As a result, the energy band gaps calculated from HOMO and LUMO levels (E_g^{CV}) are always much lower than the optical band gaps (E_g) (Table 1). This is typical for double cable

polymers, but differs from regular donor or acceptor conjugated polymers where the opposite is commonly found. Introduction of sulfur and fluorine atoms has a small effect on the HOMO and LUMO levels of the polymer, which are both lowered with respect to the vacuum level. HOMO levels of PBDTPBIs determined by ultraviolet photoelectron spectroscopy (UPS) measurement show similar trend with CV results (Figure S5 and Table 1). The effects of sulfur and fluorine on the HOMO energy levels were anticipated as they are directly attached to conjugated backbone,[34] but the effect on the LUMO levels, which are governed by the PBI units, was not expected.

2.3. Crystalline properties and phase separation in these polymers. Since DFT calculations revealed that the PBDTPBIs possess a linear conjugated backbone, it is interesting to investigate the crystallinity and the possible nanophase separation of these polymers using grazing-incidence wide-angle and small-angle X-ray scattering (GIWAXS and GISAXS) as shown in Figures 3 and 4, respectively. The polymer thin films spin-casted on Si substrates using CB solution show mixed "edge-on" and "face-on" orientation, as confirmed by their strong (100) diffraction peaks in the out-of-plane and in-plane direction (Figure S6a-c). Intensity of the (100) diffraction peaks in the out-of-plane direction are greatly reduced by adding a high boiling point diiodooctane (DIO) into spin-coating solution (Figure S6d-f). When the polymer thin films are further annealed at 150 °C, the (100) diffraction peaks in the out-of-plane direction almost disappear and at the same time (100) diffraction peaks in the in-plane direction can be observed, indicating that the conjugated backbones exhibit preferentially "face-on" orientation (Figure 3). The results reveal that the microstructure of single-component conjugated polymers strongly depends on the fabrication condition as observed in BHJ systems.

Interestingly, the introduction of PBI units switched the orientation of the conjugated backbone with respect to the substrate from "edge-on" for PBDTT (Figure 3d) to "face-on" for the PBDTPBIs (Figure 3a-c), demonstrated by the strong (100) diffraction peak in the out-of-plane direction for PBDTT, which disappeared in PBDTPBIs. This is the preferred orientation for charge transport in organic solar cells.[65] Additionally, incorporation of the PBIs resulted in distinct (010) diffraction peaks in the

out-of-plane direction, evidencing π-π stacking of the conjugated backbones or the PBI units with stacking distance of 3.63 ± 0.02 Å in a direction normal to the plane of the film.[66] In order to assign the (010) diffraction peaks to the conjugated backbone or the PBI units, we synthesize three new random copolymers, PBDTPBI-10, PBDTPBI-50 and PBDTPBI-80 with varied PBI content (Scheme 1). GIWAXS analysis shows that (010) diffraction peaks are absent in the polymer PBDTT and PBDTPBI-10, and start to be observed in PBDTPBI-50. In addition, the intensity of (010) peaks is enhanced when increasing the content of PBI units (Figure S7). These results indicate that (010) diffraction peaks in these single-component polymers can be owing to the π-π stacking of PBIs. This study also confirms that PBDTT backbone can generate ordered structures, which is helpful for PBI units to form crystalline morphology.

The large-size PBIs seemingly have little impact on the lamellar stacking of polymers, because the *d*-spacings of (100) peaks of PBDTPBIs were slightly larger or similar to that of PBDTT (Figure 3 and Table 2). With its dodecyl linker and the tricosan-12-yl swallow tail the PBI units are much larger than the 2-ethylhexyl side chain of PBDTT, and it is likely that the large PBI side units would change the lamellar spacing. In fact, the molecular weight of the repeating unit of the PBDTPBIs, consisting of two BDTs, is more than twice as large as the two BDTs in PBDTT. We therefore propose that the PBI units form a real second phase, next to the PBDTT backbone, providing a nanophase separation with a short distance between PBDTT and PBI for efficient charge separation as shown in Figure 4a. The alternating PBDTT and PBI units can explain the similar *d*-spacings for PBDTPBI and PBDTT, which would be difficult to reconcile otherwise. The nanophase separation as schematically shown in Figure 4a ensures efficient exciton dissociation into free charge carriers and provides percolating pathways for both electrons and holes.

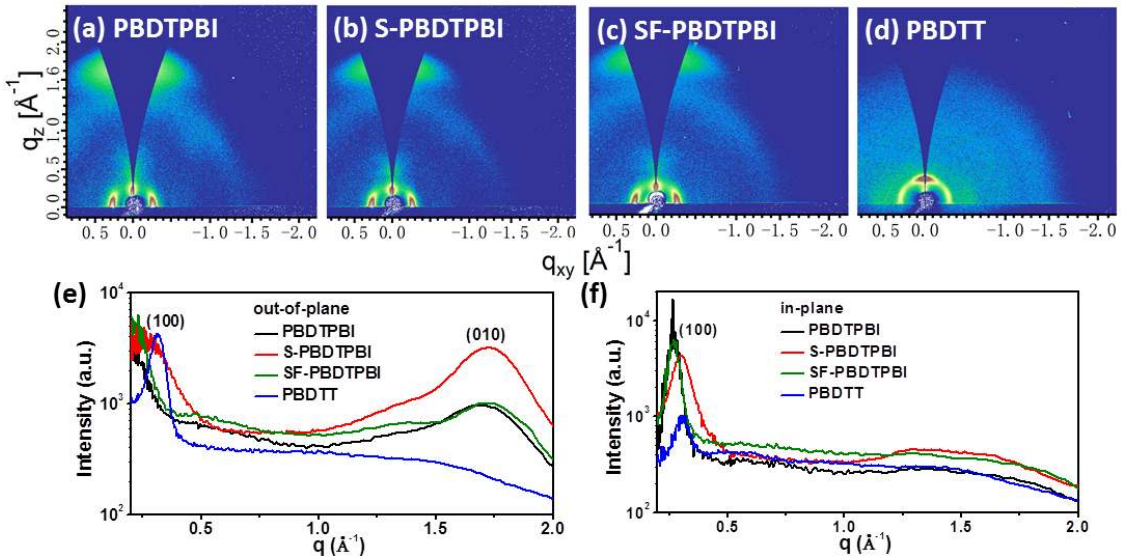

Figure 3. Characteristics of the polymer thin films spin-casted on Si substrates using CB/DIO and annealed at 150 °C for 10 min. (a-d) GIWAXS patterns, and (e) the out-of-plane and in-plane cuts of the corresponding GIWAXS patterns.

Table 2. Crystallographic Parameters of the Pure Polymers in Thin Films.

Polymer[a]	In-plane (100)		Out-of-plane (010)	
	d (Å)	CL[a] (nm)	*d* (Å)	CL[a] (nm)
PBDTPBI	23.3	13.4	3.65	2.1
S-PBDTPBI	20.3	7.7	3.61	2.5
SF-PBDTPBI	20.9	10.6	3.63	2.4
PBDTT	20.3	9.5	-	-

[a] 2CL = 2π*k*/fwhm, where *k* is a shape factor (here uses 0.9).

GISAXS (Figure 4b) reveals a characteristic distance of about 5-6 nm in these polymers, especially for SF-PBDTPBI which has a diffraction peak at $q \sim 0.13$ Å^{-1}, corresponding to a distance of about 5 nm, which is close to twice the lamellar packing inferred from GIWAXS. This is consistent with the proposed structures in Figure 4a. It is worthy mentioned that the GISAXS signal is comparatively weak which would be caused by a broad length scale distribution of the characteristic structure. We synthesized a high molecular weight SF-PBDTPBI (M_n = 33.0 kDa and M_w = 60.8 kDa) and perform the GISAXS measurement, but the intensity has no obvious change (Figure S8). It is desired

to emphasize that real morphology in the polymer thin films is complicated, such as three dimensional microstructures and the possible amorphous region. Therefore, more deep investigation into the morphology in these polymers will be required in the future.

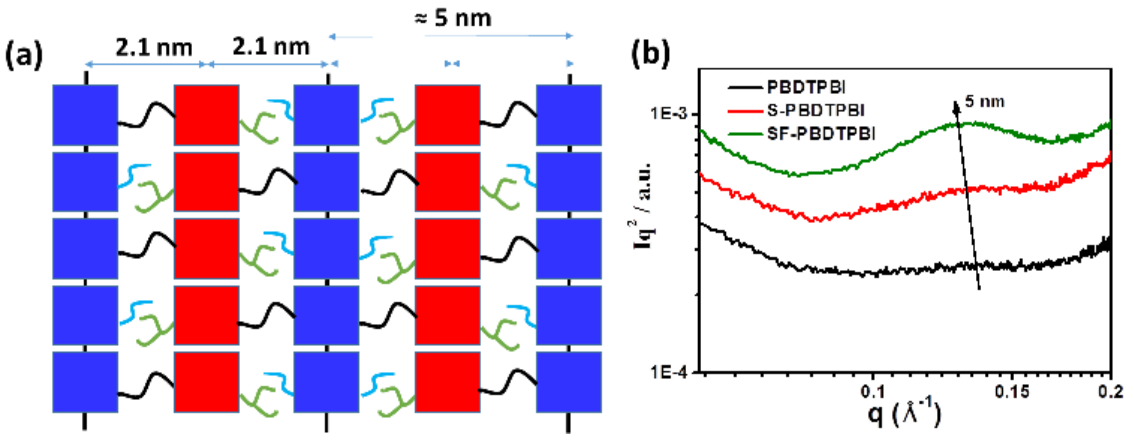

Figure 4. (a) Illustration of PBDTPBIs in nanostructures. Top view: BDT is blue color and PBI is red color. (b) GISAXS profiles of the pure polymer thin films spin-casted on Si substrates using CB/DIO and annealed at 150 °C for 10 min.

2.4. Morphology studies by AFM and TEM. We further used atomic force microscopy (AFM) and transmission electron microscopy (TEM) to study the morphology of single-component active layers (Figure 6). The AFM phase images of the PBDTPBIs show little contrast with 10 – 20 nm surface features. On the other hand, thin PBDTT:PBI BHJ films show very large phase separation (Figure S9, SI). In the bright-field TEM images of the PBDTPBIs show clear fringe patterns. By using Fourier transform, *d*-spacings of 2.41, 2.32, and 2.29 nm can be obtained from the TEM images for the three polymers, respectively. These values are close to the *d*-spacings of lamellar stacking of side units in these polymers (Table 2) determined by GIWAXS. We think *d*-spacings in TEM images are the distance between PBI and PBDTT backbone, but not the distance between two PBIs or PBDTT backbones due to the low contrast. The times the distance is close to the value from GISAXS, which is consistent with the proposed structure in Figure 4a.

In summary, the PBI side units in these double-cable polymers enable the "face-on" orientation, improved π-π stacking, and crystallinity, resulting in a nanophase

separation between PBDTT backbone and pendant PBI units. These advantages allow for efficient exciton diffusion, charge separation and transport, and meanwhile reduce charge recombination, indicating their possibility to achieve efficient solar cells.

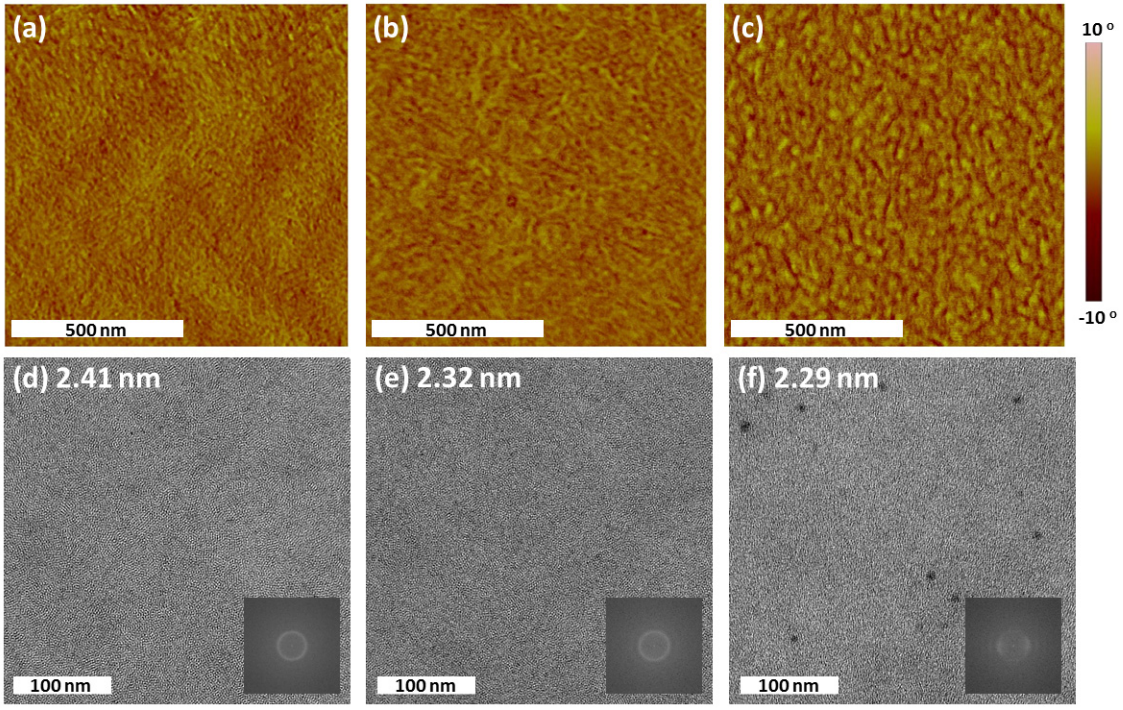

Figure 5. (a-c) AFM phase images and (d-f) bright-field TEM images of the polymer thin films fabricated from CB/DIO solution and annealed at 150 °C for 10 min. (a,d) PBDTPBI, (b,e) S-PBDTPBI, and (c,f) SF-PBDTPBI. Inserts: Fourier transform of part of the images to determine *d*-spacings.

2.5. Single-component photovoltaic performance. The new double-cable polymers were applied in SCPSCs using an inverted configuration in which ITO/ZnO and MoO_3/Ag were used as electrodes. The photoactive layers containing PBDTPBI, S-PBDTPBI, or SF-PBDTPBI were spin-coated from CB solution, in which the solvent additive, thickness of the photoactive layers, and the thermal annealing temperature were carefully optimized, as summarized in Tables S1 to S6. The use of a 1,8-diiodooctane (DIO) as high boiling point processing additive and thermal annealing at 150 °C consistently improve the photovoltaic performance, mainly due to enhanced fill factors (FFs). The improvement is possibly due to the better microstructures when using additive

and annealing process, as discussed in previous section. BHJ solar cells based on PBDTT:PBI (1:1) were also fabricated for comparison (Table S7). The *J-V* characteristics of optimized solar cells are presented in Figure 6 and the data is summarized in Table 3.

Table 3. Characteristics of Optimized Single-Component Organic Solar Cells.

Active Layer	J_{sc} (mA cm^{-2})	V_{oc} (V)	FF	PCE [a] (%)	EQE_{max}
PBDTPBI [b]	7.54 (7.25±0.18)	0.69 (0.69±0.04)	0.53 (0.51±0.02)	2.73 (2.56±0.09)	0.64
S-PBDTPBI [b]	8.05 (7.97±0.10)	0.78 (0.78±0.005)	0.57 (0.56±0.011)	3.60 (3.49±0.06)	0.67
SF-PBDTPBI [c]	7.60 (7.41±0.12)	0.92 (0.92±0)	0.60 (0.58±0.013)	4.18 (3.96±0.12)	0.66
PBDTT:PBI [d]	2.17 (2.11±0.06)	0.93 (0.93±0.01)	0.46 (0.44±0.01)	0.94 (0.87±0.04)	0.21

[a] The highest performance cells. The values in parentheses represent statistics results from 8 independent cells. [b] Fabricated from CB/DIO (1%) solution and thermally annealed at 150 °C for 10 min. [c] Fabricated from CB/DIO (0.75%) solution and thermally annealed at 150 °C for 10 min. [d] Fabricated from CB/DIO (1%) solution without thermally annealling. The thickness of all active layers is 50 nm.

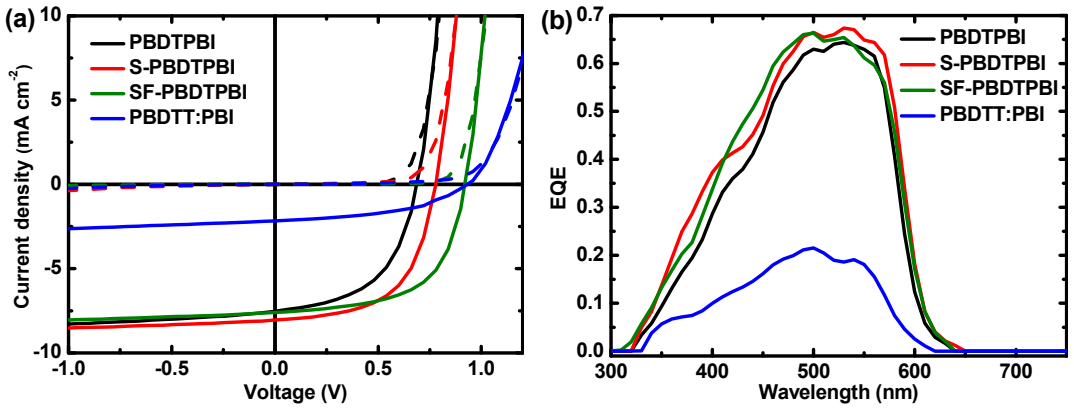

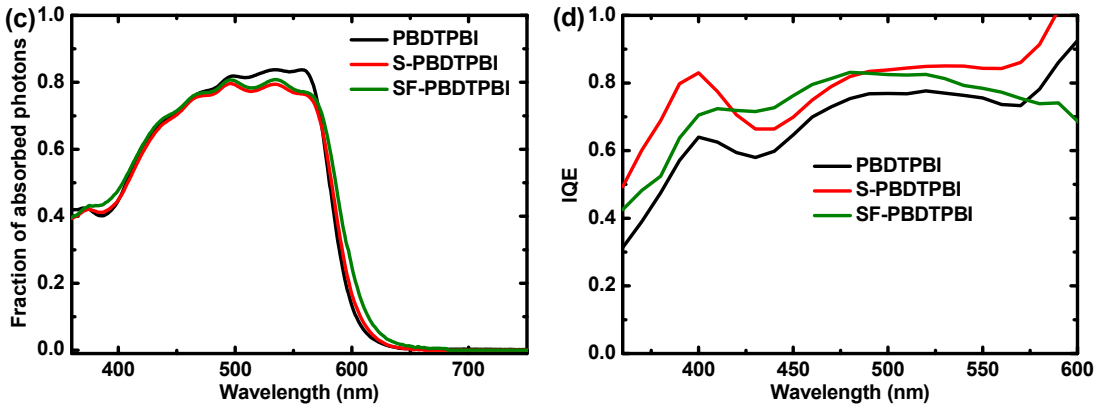

Figure 6. Characteristics of PBDTPBI, S-PBDTPBI, SF-PBDTPBI, and PBDTT:PBI (1:1 w/w) solar cells. (a) *J-V* characteristics in dark (dashed line) and under white light illumination (solid line). (b) EQE of the optimized SCOSCs. (c) Fraction of photons absorbed in the photoactive layers (50 nm for all the layers) and (d) calculated IQE spectra of SCOSCs.

The three PBDTPBI polymers exhibit a distinct photovoltaic effect with similar short-circuit current densities (J_{sc}s), while the open-circuit voltage (V_{oc}) increases in the order of PBDTPBI < S-PBDTPBI < SF-PBDTPBI. In addition to the V_{oc} increase, the FF of SCPSCs increases in the same order. This is consistent with a reduced charge recombination caused by a better nanophase separation of SF-PBDTPBI, as observed in GISAXS profiles. In contrast, the PBDTT:PBI cells show poor performance (Table 3).

The J_{sc}s of the three cells were consistent with the external quantum efficiencies (EQEs) shown in Figure 6b. All three SCPSCs show high EQEs with a maximum above 0.65. In contrast, the PBDTT:PBI cells only have an EQE below 0.21 (Table 3). We determined the internal quantum efficiencies (IQEs) of the cells by using the wavelength dependent refractive indices and extinction coefficients of all layers in the device.[67] Using these data, the fraction of absorbed photons for the active layers can be calculated (Figure 6c) via optical modeling. Although the single-component active layers only have a thickness of 50 nm, still 80% of the photons can be absorbed by the photoactive layers, which is similar to BHJs utilizing a donor polymer and acceptor molecule.[68] The IQEs (Figure 6d) were then calculated by dividing the EQEs by the fraction of absorbed photons. PBDTPBIs based active layers show IQEs above 0.60 with maximum at 0.80.

Importantly, EQEs and IQEs of SCPSCs based on PBDTPBIs are comparable to BHJ solar cells, indicating that nanophase separation between polymer backbone and PBI side chains, as inferred from GIWAXS and GISAXS, has been well-optimized. It is also worth mentioning that, PBDTPBIs have large band gaps with onset around 600 nm. This significantly limits the overlap of their absorption spectrum with the solar spectrum. Therefore, we consider that by designing new single-component conjugated polymers with extended absorption, higher power conversion efficiencies can be realized.

3. Discussion

The single-component conjugated polymers in this work provide good performance in SCOSCs, but it also leaves some questions that require further investigation. The three polymers show similar HOMO levels as indicated by CV measurement, also confirmed by ultraviolet photoelectron spectroscopy (UPS) measurement. However, they show distinct V_{oc}s in SCPSCs, from 0.69 V to 0.92 V, which is also lower than 0.93 V in PBDTT:PBI cell (Table 3). Interestingly, when reducing PBI content in the polymers, the V_{oc}s of cells can be increased from 0.69 V for PBDTPBI to 0.74 V, 0.83 V and 0.92 V for PBDTPBI-80, PBDTPBI-50 and PBDTPBI-10 (Figure S11 and Table S8), although these polymers show similar HOMO levels (Figure S10). The V_{oc} of the solar cells is related to the energy of the charge transfer state (E_{CT}) that can be studied by electroluminescence (EL) measurements (Figure 7).[69] PBDTT – based device shows strong emission at 1.8 eV, while PBDTPBI:PBI cell has strong emission at 2.0 eV that is contributed to the emission of PBI and CT emission at 1.25 eV. This is consistent with the large phase separation in PBDTPBI:PBI blend. PBDTPBI only shows CT emission at 1.25 eV, and the intensity is enhanced in S-PBDTPBI and SF-PBDTPBI. This indicates that the polymer backbones and PBI side units have better contact. SF-PBDTPBI also shows strong emission at 2.0 eV, indicating that PBI units in SF-PBDTPBI have well-organized nanostructures as in PBDTT:PBI blend. These results reveal that PBDTPBI, S-PBDTPBI and SF-PBDTPBI show distinct morphology, which would be responsible for their different V_{oc}s. However, three polymers show similar CT emission at 1.25 eV that couldn't explain the varied V_{oc}s.

Therefore, we think further studies will be required, such as their radiative and non-radiative loss, to give the deep insight into the V_{oc} of cells.

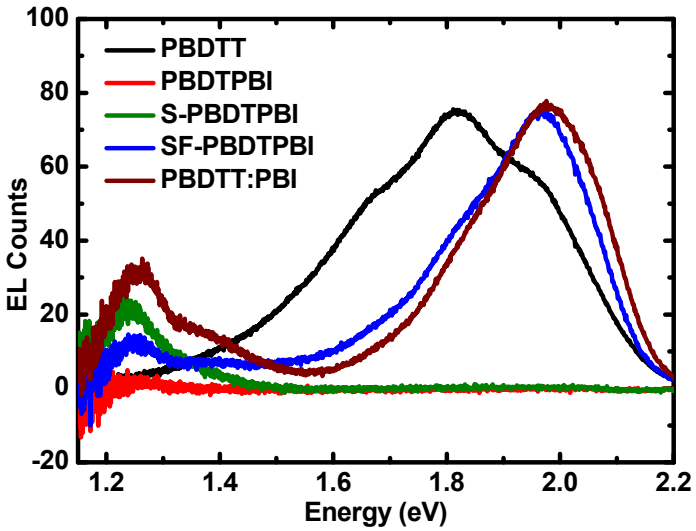

Figure 7. Normalized EL spectra of the optimized solar cells.

Another issue is about significantly increased EQEs and FF in these PBDTPBIs – based cells compared to previous DPP – based SCPSCs.[33] The EQEs in organic solar cells relate to the efficiency of exciton diffusion, charge dissociation and transport. Excitons require excess energy to be separated into free charges due to the low dielectric constant of organic semiconductors. The excess energy can be easily determined by the energy loss (E_{loss}) that is defined as the difference between optical band gap (E_g) and V_{oc}, in which E_{loss} above 0.60 eV is sufficient for charge separation. We summarize E_{loss} of six SCPSCs based on DPP and BDT – polymers in Table S9, in which both of DPP and BDT – polymers show higher/similar EQE at low E_{loss}. Therefore, it seems that the low EQEs in DPP-polymers are attributed to exciton diffusion and charge transport process. We then measure the hole and electron mobilities of SCP3 and SF-PBDTPBI based cells by space charge limit current (SCLC) method, in which SCP3 – based cells perform unbalanced hole and electron mobilities with ratio of 252 (Figure S12 and Table S10). The ratio is significantly reduced to 34 in SF-PBDTPBI based cells, corresponding to their high FFs. The unbalanced hole and electron mobilities would enhance the charge recombination, also causing low EQEs. We also notice that the much high hole mobility

in SCP3 is responsible for the unbalanced mobilities, so for DPP-based single component polymers it is essential to improve the ordered structures and electron mobility of PBIs in order to achieve high FF and EQE in SCPSCs.

4. Conclusions

A series of double-cable conjugated polymers based on linear PBDTT backbone with pendant PBI units were designed for application in single-component organic solar cells. The double-cable polymers show HOMO levels close to that of PBDTT and LUMO levels similar to that of the PBI. GIWAXS and GISAXS revealed that in thin films the double-cable polymers show a "face-on" orientation of the PBDTT backbones and PBI units, which is favorable for charge transport in organic solar cells. The X-ray diffraction and microcopy data point to a nanophase separation of the PBDTT backbone and PBI side units which assists exciton dissociation and transport of the resulting charges to the electrodes. These advantages resulted in PCEs up to 4.18%, which is one of the highest performance in single-component organic solar cells. The cells showed high EQEs up to 0.65 and IQEs up to 0.80, demonstrating an outstanding absorbed photon to collected electron conversion efficiency. Our results demonstrate that by rationally designing conjugated backbone with linear structures, optimized nanophase separation in single-component polymers can be realized, and therefore high performance single-component organic solar cells can be achieved.

Supporting Information

Materials and measurements, synthesis, TGA and DSC, absorption, CV and UPS, GIWAXS and GISAXS, AFM images, solar cells performance, SCPSCs comparison between DPP and BDT, and NMR spectra. This material is available free of charge via the Internet at http://pubs.acs.org.

Author Information

Corresponding Author

E-mail: liweiwei@iccas.ac.cn

Notes

The authors declare no competing financial interest

Acknowledgement

We thank Yanxi Zhang from the University of Groningen for fruitful discussion and suggestion. This study is jointly supported by MOST (2017YFA0204702) and NSFC (51773207, 21574138, 51603209, 91633301) of China. This work was further supported by the Strategic Priority Research Program (XDB12030200) of the Chinese Academy of Sciences and the Recruitment Program of Global Youth Experts of China. The research also received funding from the European Research Council (ERC Grant Agreement No. 339031) and from the Ministry of Education, Culture and Science (Gravity program 024.001.035). ML acknowledges funding from the European Union's Horizon 2020 research and innovation programme under the Marie Skłodowska-Curie grant agreement No. 747422.

References

(1) Cravino, A.; Sariciftci, N. S. *J. Mater. Chem.* **2002**, *12*, 1931.

(2) Roncali, J. *Chem. Soc. Rev.* **2005**, *34*, 483.

(3) Sommer, M.; Huettner, S.; Thelakkat, M. *J. Mater. Chem.* **2010**, *20*, 10788.

(4) Roncali, J. *Adv. Energy Mater.* **2011**, *1*, 147.

(5) Wang, J.; Higashihara, T. *Polym. Chem.* **2013**, *4*, 5518.

(6) Blom, P. W. M.; Mihailetchi, V. D.; Koster, L. J. A.; Markov, D. E. *Adv. Mater.* **2007**, *19*, 1551.

(7) Nguyen, T. L.; Lee, T. H.; Gautam, B.; Park, S. Y.; Gundogdu, K.; Kim, J. Y.; Woo, H. Y. *Adv. Funct. Mater.* **2017**, *27*, 1702474.

(8) Guo, C.; Lin, Y.-H.; Witman, M. D.; Smith, K. A.; Wang, C.; Hexemer, A.; Strzalka, J.; Gomez, E. D.; Verduzco, R. *Nano Lett.* **2013**, *13*, 2957.

(9) Wang, J.; Ueda, M.; Higashihara, T. *ACS Macro Lett.* **2013**, *2*, 506.

(10) Lombeck, F.; Komber, H.; Sepe, A.; Friend, R. H.; Sommer, M. *Macromolecules* **2015**, *48*, 7851.

(11) Wang, S.; Yang, Q.; Tao, Y.; Guo, Y.; Yang, J.; Liu, Y.; Zhao, L.; Xie, Z.; Huang, W. *New J. Chem.* **2016**, *40*, 1825.

(12) Brady, M. A.; Ku, S.-Y.; Perez, L. A.; Cochran, J. E.; Schmidt, K.; Weiss, T. M.; Toney, M. F.; Ade, H.; Hexemer, A.; Wang, C.; Hawker, C. J.; Kramer, E. J.; Chabinyc, M. L. *Macromolecules* **2016**, *49*, 8187.

(13) Lombeck, F.; Sepe, A.; Thomann, R.; Friend, R. H.; Sommer, M. *ACS Nano* **2016**, *10*, 8087.

(14) Nübling, F.; Komber, H.; Sommer, M. *Macromolecules* **2017**, *50*, 1909.

(15) Lee, D. H.; Lee, J. H.; Kim, H. J.; Choi, S.; Park, G. E.; Cho, M. J.; Choi, D. H. *J. Mater. Chem. A* **2017**, *5*, 9745.

(16) Grieco, C.; Aplan, M. P.; Rimshaw, A.; Lee, Y.; Le, T. P.; Zhang, W.; Wang, Q.; Milner, S. T.; Gomez, E. D.; Asbury, J. B. *J. Phys. Chem. C* **2016**, *120*, 6978.

(17) Tao, Y.; McCulloch, B.; Kim, S.; Segalman, R. A. *Soft Matter* **2009**, *5*, 4219.

(18) Yang, C.; Lee, J. K.; Heeger, A. J.; Wudl, F. *J. Mater. Chem.* **2009**, *19*, 5416.

(19) Hufnagel, M.; Fischer, M.; Thurn-Albrecht, T.; Thelakkat, M. *Polym. Chem.* **2015**, *6*, 813.

(20) Raissi, M.; Erothu, H.; Ibarboure, E.; Bejbouji, H.; Cramail, H.; Cloutet, E.; Vignau, L.; Hiorns, R. C. *J. Mater. Chem. A* **2017**, *5*, 7533.

(21) Hiorns, R. C.; Cloutet, E.; Ibarboure, E.; Khoukh, A.; Bejbouji, H.; Vignau, L.; Cramail, H. *Macromolecules* **2010**, *43*, 6033.

(22) Zhang, Q.; Cirpan, A.; Russell, T. P.; Emrick, T. *Macromolecules* **2009**, *42*, 1079.

(23) Zhang, F.; Svensson, M.; Andersson, M. R.; Maggini, M.; Bucella, S.; Menna, E.; Inganäs, O. *Adv. Mater.* **2001**, *13*, 1871.

(24) Ramos, A. M.; Rispens, M. T.; van Duren, J. K. J.; Hummelen, J. C.; Janssen, R. A. J. *J. Am. Chem. Soc.* **2001**, *123*, 6714.

(25) Giacalone, F.; Segura, J. L.; Martín, N.; Catellani, M.; Luzzati, S.; Lupsac, N. *Org. Lett.* **2003**, *5*, 1669.

(26) Tan, Z.; Hou, J.; He, Y.; Zhou, E.; Yang, C.; Li, Y. *Macromolecules* **2007**, *40*, 1868.

(27) Koyuncu, S.; Zafer, C.; Koyuncu, F. B.; Aydin, B.; Can, M.; Sefer, E.; Ozdemir, E.; Icli, S. *J. Polym. Sci., Part A: Polym. Chem.* **2009**, *47*, 6280.

(28) Gholamkhass, B.; Peckham, T. J.; Holdcroft, S. *Polym. Chem.* **2010**, *1*, 708.

(29) Miyanishi, S.; Zhang, Y.; Hashimoto, K.; Tajima, K. *Macromolecules* **2012**, *45*, 6424.

(30) Yamamoto, S.; Yasuda, H.; Ohkita, H.; Benten, H.; Ito, S.; Miyanishi, S.; Tajima, K.; Hashimoto, K. *J. Phys. Chem. C* **2014**, *118*, 10584.

(31) Pierini, F.; Lanzi, M.; Nakielski, P.; Pawłowska, S.; Urbanek, O.; Zembrzycki, K.; Kowalewski, T. A. *Macromolecules* **2017**, *50*, 4972.

(32) Chen, P.; Nakano, K.; Suzuki, K.; Hashimoto, K.; Kikitsu, T.; Hashizume, D.; Koganezawa, T.; Tajima, K. *ACS Appl. Mater. Interfaces* **2017**, *9*, 4758.

(33) Lai, W.; Li, C.; Zhang, J.; Yang, F.; Colberts, F. J. M.; Guo, B.; Wang, Q. M.; Li, M.; Zhang, A.; Janssen, R. A. J.; Zhang, M.; Li, W. *Chem. Mater.* **2017**, *29*, 7073.

(34) Zhao, W.; Li, S.; Yao, H.; Zhang, S.; Zhang, Y.; Yang, B.; Hou, J. *J. Am. Chem. Soc.* **2017**, *139*, 7148.

(35) Huang, Y.; Kramer, E. J.; Heeger, A. J.; Bazan, G. C. *Chem. Rev.* **2014**, *114*, 7006.

(36) McNeill, C. R.; Abrusci, A.; Hwang, I.; Ruderer, M. A.; Müller-Buschbaum, P.; Greenham, N. C. *Adv. Funct. Mater.* **2009**, *19*, 3103.

(37) Park, S. K.; Kim, Y. H.; Han, J. I. *Jpn. J. Appl. Phys.* **2009**, *48*.

(38) McNeill, C. R. *Energy Environ. Sci.* **2012**, *5*, 5653.

(39) Tamai, Y.; Ohkita, H.; Benten, H.; Ito, S. *J. Phys. Chem. Lett.* **2015**, *6*, 3417.

(40) Li, W.; Hendriks, K. H.; Roelofs, W. S. C.; Kim, Y.; Wienk, M. M.; Janssen, R. A. J. *Adv. Mater.* **2013**, *25*, 3182.

(41) Kim, K.; Liu, J.; Namboothiry, M. A. G.; Carroll, D. L. *Appl. Phys. Lett.* **2007**, *90*.

(42) Li, W.; Hendriks, K. H.; Furlan, A.; Roelofs, W. S. C.; Wienk, M. M.; Janssen, R. A. J. *J. Am. Chem. Soc.* **2013**, *135*, 18942.

(43) Nguyen, T. L.; Choi, H.; Ko, S. J.; Uddin, M. A.; Walker, B.; Yum, S.; Jeong, J. E.; Yun, M. H.; Shin, T. J.; Hwang, S.; Kim, J. Y.; Woo, H. Y. *Energy Environ. Sci.* **2014**, *7*, 3040.

(44) Jiang, J.-M.; Yuan, M.-C.; Dinakaran, K.; Hariharan, A.; Wei, K.-H. *J. Mater. Chem. A* **2013**, *1*, 4415.

(45) Viterisi, A.; Gispert-Guirado, F.; Ryan, J. W.; Palomares, E. *J. Mater. Chem.* **2012**, *22*, 15175.

(46) Dutta, P.; Park, H.; Lee, W. H.; Kang, I. N.; Lee, S. H. *Org. Electron.* **2012**, *13*, 3183.

(47) Zhang, Q.; Kelly, M. A.; Bauer, N.; You, W. *Acc. Chem. Res.* **2017**, *50*, 2401.

(48) Li, W.; Hendriks, K. H.; Furlan, A.; Roelofs, W. S. C.; Meskers, S. C. J.; Wienk, M. M.; Janssen, R. A. J. *Adv. Mater.* **2014**, *26*, 1565.

(49) van Franeker, J. J.; Heintges, G. H. L.; Schaefer, C.; Portale, G.; Li, W.; Wienk, M. M.; van der Schoot, P.; Janssen, R. A. J. *J. Am. Chem. Soc.* **2015**, *137*, 11783.

(50) Zhou, E.; Cong, J.; Hashimoto, K.; Tajima, K. *Adv. Mater.* **2013**, *25*, 6991.

(51) Collins, B. A.; Tumbleston, J. R.; Ade, H. *J. Phys. Chem. Lett.* **2011**, *2*, 3135.

(52) Zhang, C.; Langner, S.; Mumyatov, A. V.; Anokhin, D. V.; Min, J.; Perea, J. D.; Gerasimov, K. L.; Osvet, A.; Ivanov, D. A.; Troshin, P.; Li, N.; Brabec, C. J. *J. Mater. Chem. A* **2017**, *5*, 17570.

(53) Hartmeier, B. F.; Brady, M. A.; Treat, N. D.; Robb, M. J.; Mates, T. E.; Hexemer, A.; Wang, C.; Hawker, C. J.; Kramer, E. J.; Chabinyc, M. L. *J. Polym. Sci., Part B: Polym. Phys.* **2016**, *54*, 237.

(54) Peet, J.; Kim, J. Y.; Coates, N. E.; Ma, W. L.; Moses, D.; Heeger, A. J.; Bazan, G. C. *Nat. Mater.* **2007**, *6*, 497.

(55) Ma, W. L.; Yang, C. Y.; Gong, X.; Lee, K.; Heeger, A. J. *Adv. Funct. Mater.* **2005**, *15*, 1617.

(56) Yang, X. N.; Loos, J.; Veenstra, S. C.; Verhees, W. J. H.; Wienk, M. M.; Kroon, J. M.; Michels, M. A. J.; Janssen, R. A. J. *Nano Lett.* **2005**, *5*, 579.

(57) Tang, H.; Lu, G.; Li, L.; Li, J.; Wang, Y.; Yang, X. *J. Mater. Chem.* **2010**, *20*, 683.

(58) Yassar, A.; Miozzo, L.; Gironda, R.; Horowitz, G. *Prog. Polym. Sci.* **2013**, *38*, 791.

(59) Loewe, R. S.; Ewbank, P. C.; Liu, J. S.; Zhai, L.; McCullough, R. D. *Macromolecules* **2001**, *34*, 4324.

(60) Sheina, E. E.; Liu, J.; Iovu, M. C.; Laird, D. W.; McCullough, R. D. *Macromolecules* **2004**, *37*, 3526.

(61) Miyakoshi, R.; Yokoyama, A.; Yokozawa, T. *J. Am. Chem. Soc.* **2005**, *127*, 17542.

(62) Beryozkina, T.; Senkovskyy, V.; Kaul, E.; Kiriy, A. *Macromolecules* **2008**, *41*, 7817.

(63) Liang, N.; Jiang, W.; Hou, J.; Wang, Z. *Mater. Chem. Front.* **2017**, *1*, 1291.

(64) Kang, T. E.; Kim, T.; Wang, C.; Yoo, S.; Kim, B. J. *Chem. Mater.* **2015**, *27*, 2653.

(65) Vohra, V.; Kawashima, K.; Kakara, T.; Koganezawa, T.; Osaka, I.; Takimiya, K.; Murata, H. *Nat Photon* **2015**, *9*, 403.

(66) Nolde, F.; Pisula, W.; Müller, S.; Kohl, C.; Müllen, K. *Chem. Mater.* **2006**, *18*, 3715.

(67) Gilot, J.; Wienk, M. M.; Janssen, R. A. J. *Adv. Mater.* **2010**, *22*, E67.

(68) Li, W.; Roelofs, W. S. C.; Wienk, M. M.; Janssen, R. A. J. *J. Am. Chem. Soc.* **2012**, *134*, 13787.

(69) Zhou, Y.; Tvingstedt, K.; Zhang, F. L.; Du, C. X.; Ni, W. X.; Andersson, M. R.; Inganäs, O. *Adv. Funct. Mater.* **2009**, *19*, 3293.

Graphical Abstract for ToC